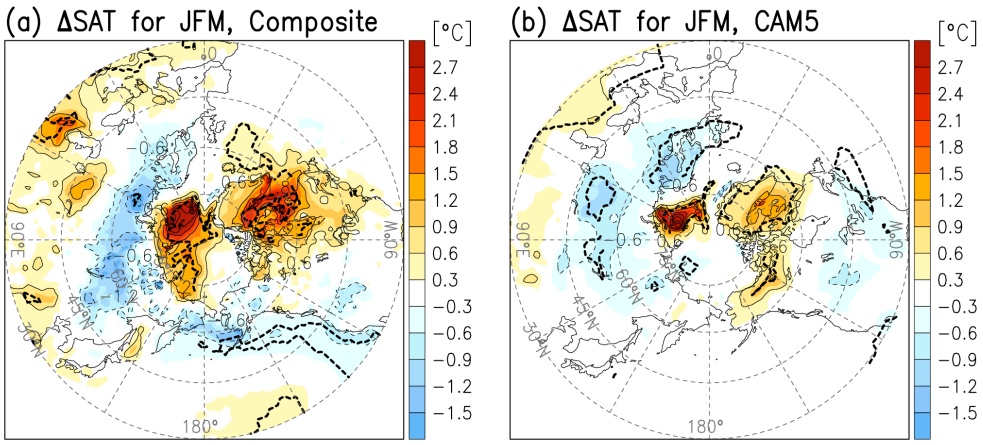

Supplementary Figure 1 | Changes in surface air temperatures during the late winter months. (a) Identical calculations as in Fig. 2a for late winter. **(b)** Identical calculations as in Fig. 3a for late winter. In both figures, the contour interval is 0.3 °C and values that are statistically significant at the 95 % confidence level are enclosed by a dotted line (see Methods).

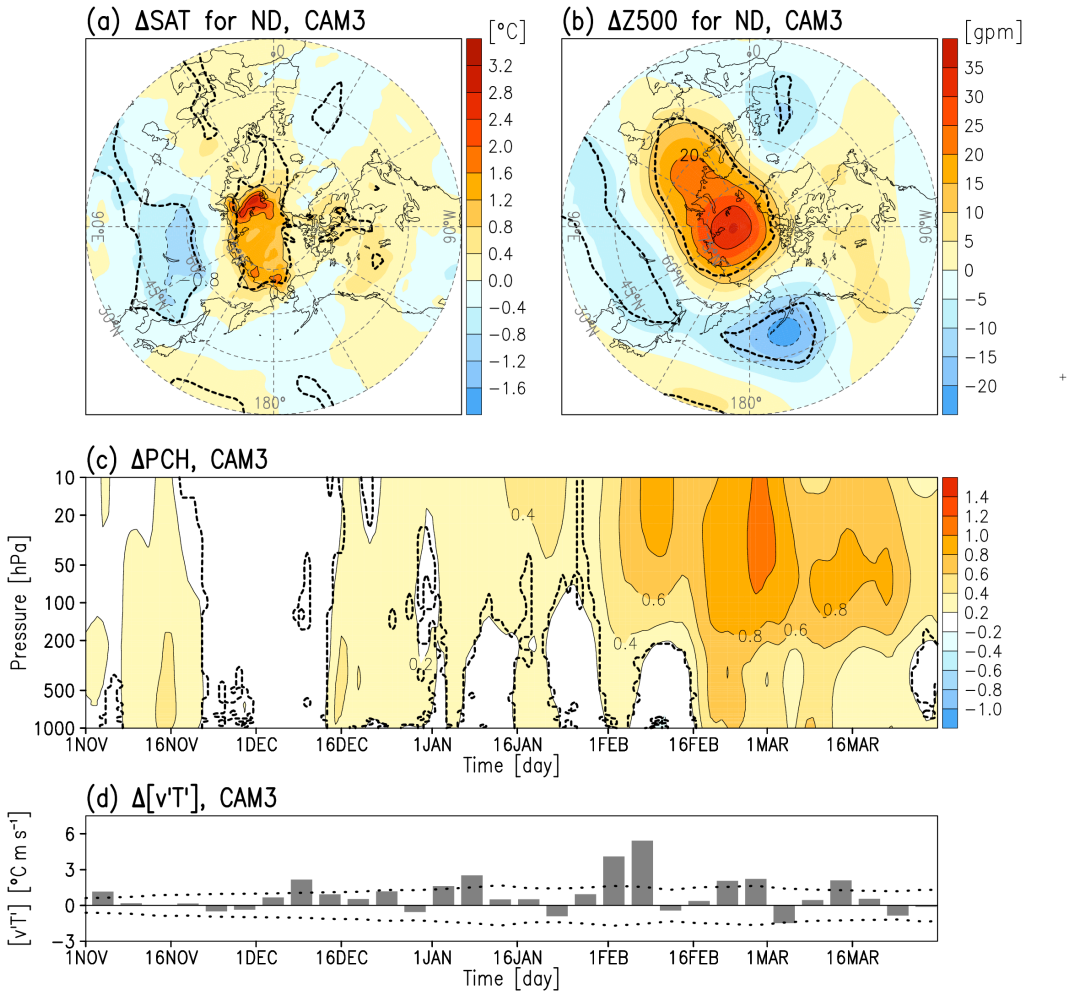

Supplementary Figure 2 | Model ensembles mean response for the reduced Arctic sea ice condition (CAM3 results). Model ensemble mean responses to the reduced SIC over B-K seas for **(a)** surface air temperature, **(b)** the geopotential height anomaly at 500 hPa for the early winter, **(c)** the subseasonal evolution of the PCH as a function of pressure, and **(d)** 5-day averaged poleward heat flux anomalies at 100 hPa. In **(a)** and **(b)**, contour intervals are 0.4 °C and 5 m, respectively. In **(c)**, the contour interval is 0.2. Values that are statistically significant at the 95% confidence level are enclosed by a dotted line (see Methods).

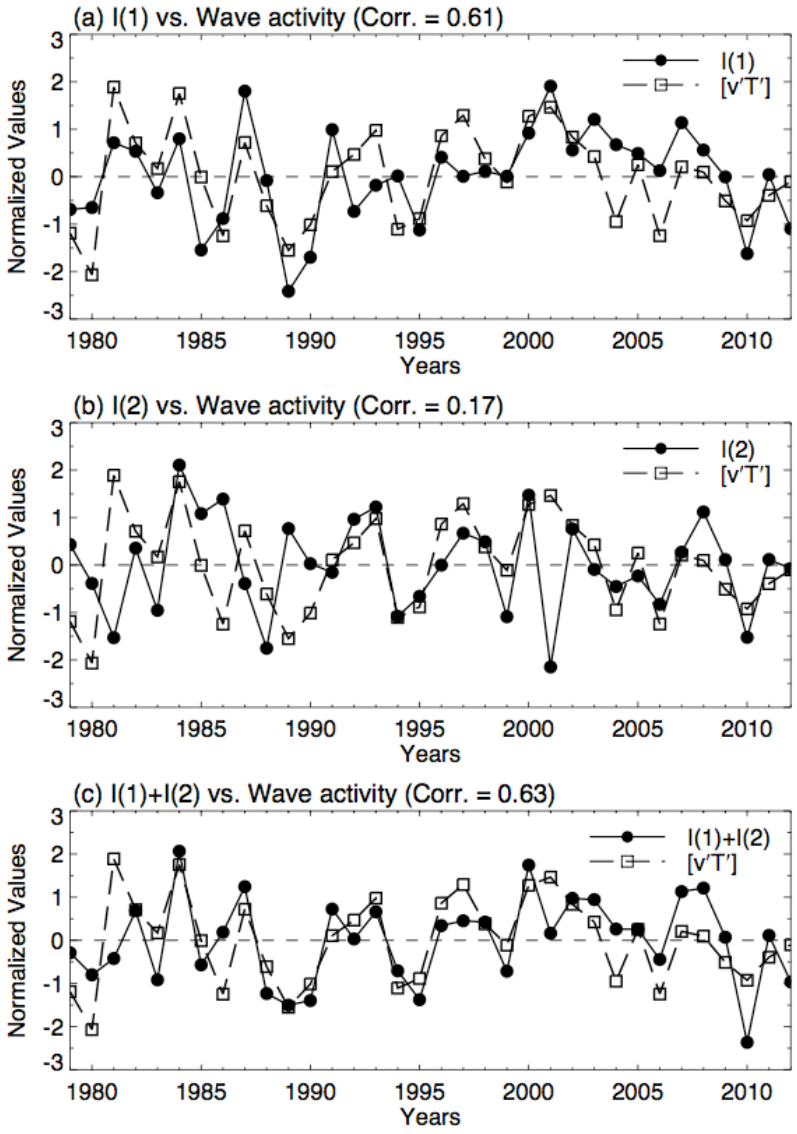

Supplementary Figure 3 | Vertical wave activity explained by linear interference. Interference index (filled circles with solid-line borders) and vertical wave activity, [*v'T'*], at 100-hPa (unfilled squares with dashed-line borders) during the early winter months averaged over 45°N to 75°N for **(a)** wavenumber 1, **(b)** wavenumber 2, and **(c)** wavenumbers 1 and 2. The interference index, the degree of linear interference for early winter season of each year (1979-2012), was obtained by projecting the anomalous planetary-scale wave for early winter onto the climatological wave. The calculation was conducted for each wavenumber. Here, the interference of wavenumber k is

defined as $I(k) = \sum_{n} \bar{\Phi}_{n,k} \Phi'_{n,k} \cos\theta$, where k denotes wavenumber 1 or 2. θ is latitude. $\overline{\Phi}_{n,k}$ is the climatological 300 hPa geopotential height of wavenumber 1 or 2, and $\Phi'_{n,k}$ is the anomaly deviating from the climatology data. The summation is applied to each grid point n within the latitudinal band of 45°N to 75°N to obtain the projection of $\Phi'_{n,k}$ onto $\overline{\Phi}_{n,k}$ within the active wave propagation region. Given that $\overline{\Phi}_{n,k}$ interference depends on both the amplitude of $\Phi'_{n,k}$ and the phase difference of $\Phi'_{n,k}$ from $\overline{\Phi}_{n,k}$. To provide a comparison, each time-series is normalized by the standard deviation.

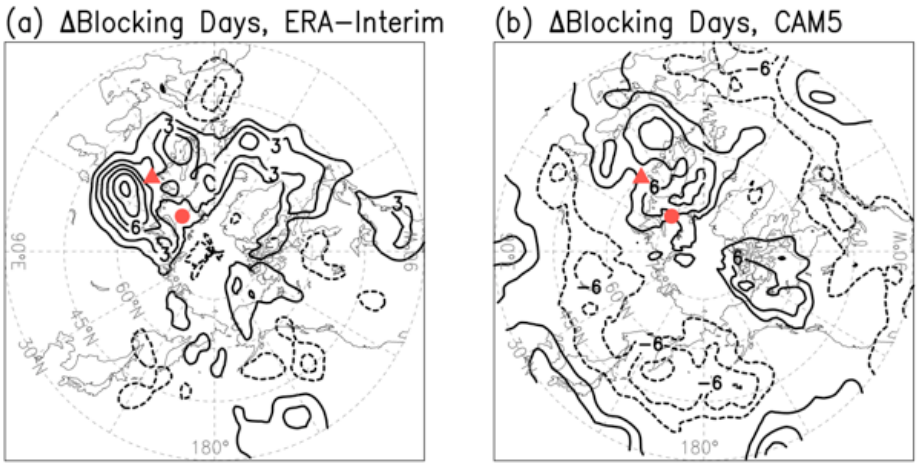

Supplementary Figure 4 | Blocking frequency changes associated with Arctic sea ice loss. (a) Differences between mean blocking days during the early winter for normal years and years of reduced sea ice indicated by red dots in Fig. 1a. **(b)** Same calculation with (a) applied to the model simulations: i.e. differences between the control and perturbed simulations. Key locations of troposphere-stratosphere linkages addressed in the literature (Supplementary ref. 1 and ref. 2) are denoted by the filled circle and filled triangle, respectively. For each grid point, an individual blocking event is identified by tracking a 500-hPa synoptic-scale height anomaly that exceeds one standard deviation from its mean for a minimum of five consecutive days (Supplementary ref. 3).

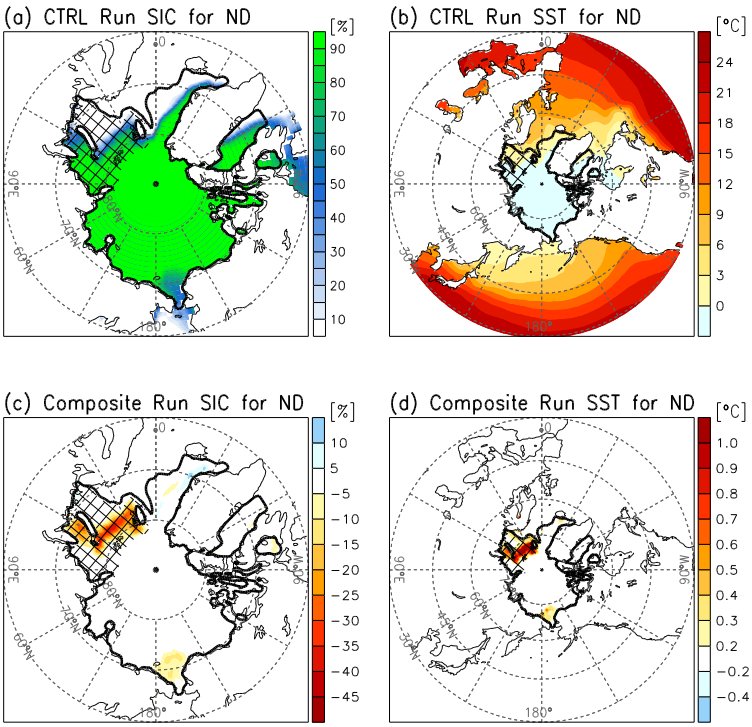

Supplementary Figure 5 | Sea ice and SST boundary conditions for model simulation. Spatial patterns of **(a)** SIC and **(b)** SST climatological boundary conditions used for the control run. **(c)** SIC and **(d)** SST composite mean anomalies obtained by averaging the selected years (red dots) shown in Fig. 1a (denoted by red dots). The perturbed run is integrated with the anomalies that are added to the climatology data (e.g., (a)+(c) for SIC and (b)+(d) for SST). Although the early winter seasonal average is shown here to provide a visual representation, the boundary condition for each experiment is prepared for entire one year cycle. The Arctic Ocean boundary is marked by the solid line (see Methods), and the B-K seas are marked by the hatched region.

Supplementary References

1. Nishii, K., Nakamura, H. & Orsolini, Y. J. Geographical Dependence Observed in Blocking High Influence on the Stratospheric Variability through Enhancement and Suppression of Upward Planetary-Wave Propagation. *J. Clim.* **24,** 6408–6423 (2011).

2. Garfinkel, C. I., Hartmann, D. L. & Sassi, F. Tropospheric Precursors of Anomalous Northern Hemisphere Stratospheric Polar Vortices. *J. Clim.* **23,** 3282–3299 (2010).

3. Dole, R. M. & Gordon, N. D. Persistent Anomalies of the Extratropical Northern Hemisphere Wintertime Circulation: Geographical Distribution and Regional Persistence Characteristics. *Mon. Weather Rev.* **111,** 1567–1586 (1983).